

# Nonlinear dynamics of a cigar-shaped Bose-Einstein condensate in an optical cavity

J. M. Zhang, F. C. Cui, D. L. Zhou, and W. M. Liu

*Beijing National Laboratory for Condensed Matter Physics, Institute of Physics, Chinese Academy of Sciences, Beijing 100080, China*

(Received 3 December 2008; published 3 March 2009)

We investigate the nonlinear dynamics of a combined system which is composed of a cigar-shaped Bose-Einstein condensate and an optical cavity with the two sides coupled dispersively. This system is characterized by the cavity-induced nonlinearity; after integrating out the fast degree of freedom of the cavity mode, the potential felt by the condensate depends on the condensate itself. Adopting a discrete-mode approximation for the condensate, we map out the steady configurations of the system. It is found that due to the nonlinearity of the system, the nonlinear levels of the system may fold up in some parameter regimes. That will lead to the breakdown of adiabatic evolution of the system. Analysis of the dynamical stability of the steady states indicates that the same level structure also results in optical bistability.

DOI: [10.1103/PhysRevA.79.033401](https://doi.org/10.1103/PhysRevA.79.033401)

PACS number(s): 37.10.Jk, 37.10.Vz, 42.50.Pq, 42.65.Pc

## I. INTRODUCTION

Recently, a lot of investigations have been devoted to the combination of ultracold atom physics and cavity quantum electrodynamics. Experimentally, the efforts culminate in the successful coupling of a Bose-Einstein condensate (BEC), that is, a single matter-wave field mode, to a single cavity mode in a high finesse optical cavity [1,2]. Though of a very short history, this type of combined system has demonstrated many interesting phenomena, such as vacuum Rabi splitting [1,2],  $\sqrt{N}$  scaling of the atom-photon coupling [1,2], optical bistability [3,4], cavity-enhanced super-radiance of a BEC [5], and most surprisingly, a map between the atom ensemble-cavity system and the canonical optomechanical system is found [6,7]. Besides playing an active role in the dynamics, the cavity can also be utilized to characterize the properties of the matter-wave field. It has been experimentally implemented to study the statistics of an atom laser by detecting single atoms falling through a cavity [8]. Based on similar principles, proposals to probe the atomic number statistics in optical lattices so as to differentiate different quantum phases are brought up [9,10].

One of the most remarkable characteristics of the atom ensemble-cavity system is its intrinsic nonlinearity. If we are only interested in the mechanical motion of the atoms and thus restrict to the large detuning limit, the atom-photon interaction is of a dispersive nature. The atom-photon interaction provides a potential (an optical lattice) to the atoms, and meanwhile shifts the cavity mode frequency. By shifting the cavity mode frequency, the atom ensemble can influence or even determine the potential acting on itself. This entails a nonlinearity substantially different than the usual atom-atom interactions. It is this nonlinearity that lies at the heart of previous experimental and theoretical works [3,6,7,11–14], in particular, the dispersive optical bistability [3,11].

Along this line, we consider the nonlinear dynamics of a cigar-shaped Bose-Einstein condensate in an optical cavity in this work. Experimentally, this has been achieved (though not a cigar-shaped BEC) and investigated by Brennecke *et al.* [7], with the main finding that in the weak atom-atom interaction and weak excitation (or nondepletion) limit, the

condensate-cavity system maps onto the generic cavity optomechanical system perfectly. In this work we approach the same problem from the perspective of diffraction of matter wave by an optical lattice. We will not restrict to the weak excitation limit. We will develop a discrete-mode approximation (DMA) for the condensate with the idea that the dynamics of the condensate confines to some discrete modes. By comparing with the full description of Gross-Pitaevskii (GP) equation, we find that the finite-mode approximation is quantitatively good in the case of weak atom-atom interaction. The DMA also enables us to find out the steady states of the system, analyze their stability, and elucidate the possibility of breakdown of adiabaticity and optical bistability in this system.

This paper is organized as follows. In Sec. II, the system and the general formalism are described. In particular, the discrete-mode approximation is introduced. Then in Sec. III A, we compare the DMA with the full GP dynamics so as to validate it. On this basis, in Sec. III B, we address the problem of adiabatic evolution of the system, which is relevant to optical bistability. Our results are summarized in Sec. IV.

## II. GENERAL FORMALISM

We assume that a cigar-shaped Bose-Einstein condensate is located inside an optical cavity with its axial direction parallel to that of the cavity. The internal transition frequency of the two-level atoms is  $\omega_a$ , while the relevant cavity mode interacting with the atoms is of frequency  $\omega_c$ . The cavity mode is coherently driven by a pump laser with frequency  $\omega_p$  and a possibly time-dependent amplitude  $\eta(t)$ . The atom-pump and cavity-pump detunings are denoted as  $\Delta_a = \omega_a - \omega_p$  and  $\Delta_c = \omega_c - \omega_p$ , respectively. In the large detuning limit and by transferring into the rotating frame at the pump frequency, we get the Hamiltonian for the condensate-cavity system ( $\hbar = 1$  throughout this paper) [7],

$$H = \int dx \hat{\Psi}^\dagger(x) \left[ -\frac{1}{2m} \frac{d^2}{dx^2} + V_{\text{ext}}(x) + U_0 \hat{a}^\dagger \hat{a} \cos^2(kx) + \frac{g_{1D}}{2} \hat{\Psi}^\dagger(x) \hat{\Psi}(x) \right] \hat{\Psi}(x) + \Delta_c \hat{a}^\dagger \hat{a} + \eta(t)(\hat{a} + \hat{a}^\dagger) + H_\kappa. \quad (1)$$

Here,  $\hat{\Psi}^\dagger$  and  $\hat{a}^\dagger$  are the creation operators for the atoms (with mass  $m$ ) and the cavity photons, respectively.  $V_{\text{ext}}(x) = \frac{1}{2}m\omega_{\parallel}^2x^2$  is the harmonic potential in the axial direction with characteristic frequency  $\omega_{\parallel}$  and  $g_{1D}$  is the effective atom-atom interaction strength in a transversely tight-confining trap [15]. Besides the harmonic potential  $V_{\text{ext}}$  (which may also owe to atom-photon interaction, as in an optical trap), the atom-cavity photon interaction provides an additional potential  $U_0\hat{a}^\dagger\hat{a}\cos^2(kx)$  for the atoms. The difference is that the former is static, while the latter, being proportional to the intracavity photon number, may be dynamical and quantized [16]. Here  $U_0 = -g_0^2/\Delta_c$  is the maximal light shift per photon that an atom may experience (at an antinode), with  $g_0$  being the atom-photon coupling constant. Note that we assume that the transverse radius of the condensate is much smaller than the cavity mode waist, and therefore it is legitimate to neglect the variation in  $g_0$  in the transverse direction. The cavity mode function in the axial direction is  $\cos(kx)$ , with the wave vector  $k=2\pi/\lambda$ . Finally,  $H_{\kappa}$  accounts for cavity photon decay with a rate  $\kappa$ .

In the mean-field approximation, we take  $\hat{\Psi}(x,t) \sim \Psi(x,t)$  and  $\hat{a} \sim \alpha$ , i.e., both the matter-wave field and the electromagnetic field are described as classical fields. The GP equation for the condensate is

$$i\frac{\partial\Psi(x,t)}{\partial t} = \left[ -\frac{1}{2m}\frac{d^2}{dx^2} + V_{\text{ext}}(x) + U_0|\alpha|^2\cos^2(kx) + g_{1D}|\Psi(x,t)|^2 \right] \Psi(x,t), \quad (2)$$

and the equation of motion for the cavity field is

$$\frac{\partial\alpha}{\partial t} = -i \left[ \Delta_c + U_0 \int dx |\Psi(x,t)|^2 \cos^2(kx) \right] \alpha - \kappa\alpha + \eta(t). \quad (3)$$

We can numerically integrate these coupled equations so as to study the dynamics of the combined system. To this end, technically, we had better convert the original equations into their dimensionless form. The characteristic length scale and energy scale of the system are  $\xi = \lambda/2\pi$  and  $\omega_r = k^2/2m$ , i.e., the period of the optical lattice divided by  $\pi$  and the atomic recoil energy, respectively. We thus rescale position and time as  $x = \tilde{x}\xi$  and  $t = \tilde{t}/\omega_r$ , respectively, and accordingly the condensate wave function  $\Psi(x,t) = \sqrt{N/\xi}\tilde{\Psi}(\tilde{x},\tilde{t})$  so that the scaled wave function is normalized to unity,  $\int d\tilde{x} |\tilde{\Psi}(\tilde{x},\tilde{t})|^2 = 1$ . Here  $N$  is the total atom number. Equations (2) and (3) then convert to

$$i\frac{\partial\tilde{\Psi}(\tilde{x},\tilde{t})}{\partial\tilde{t}} = \left[ -\frac{d^2}{d\tilde{x}^2} + \omega^2\tilde{x}^2 + \tilde{U}_0|\alpha|^2\cos^2\tilde{x} + g|\tilde{\Psi}(\tilde{x},\tilde{t})|^2 \right] \tilde{\Psi}(\tilde{x},\tilde{t}), \quad (4)$$

$$\frac{\partial\alpha}{\partial\tilde{t}} = -i \left[ \tilde{\Delta}_c + N\tilde{U}_0 \int d\tilde{x} |\tilde{\Psi}(\tilde{x},\tilde{t})|^2 \cos^2\tilde{x} \right] \alpha - \tilde{\kappa}\alpha + \tilde{\eta}(t). \quad (5)$$

Here we introduced the rescaled dimensionless quantities  $(\tilde{U}_0, \tilde{\Delta}_c, \tilde{\kappa}, \tilde{\eta}) = (U_0, \Delta_c, \kappa, \eta)/\omega_r$ , the rescaled harmonic frequency  $\omega = \sqrt{m\omega_{\parallel}^2\xi^2/2\omega_r}$ , and the atom-atom interaction strength  $g = Ng_{1D}/\omega_r\xi$ .

At this point, a further simplification is possible. Note that experimentally the cavity damping is much faster than the mechanical motion of the condensate. The former occurs at a rate of  $\kappa$ , while the latter, roughly speaking, is on the order of  $\omega_r$  (see the discrete-mode approximation below). In the experiment of Brennecke *et al.* [7],  $\kappa = 2\pi \times 1.3$  MHz and  $\omega_r$  is around  $2\pi \times 3.75$  kHz ( $^{87}\text{Rb}$ ) so the cavity decay is almost 3 orders of magnitude faster than the condensate motion. We thus can safely assume that the cavity field follows the condensate adiabatically and solve the photon number as

$$n_{\text{ph}} = |\alpha(t)|^2 = \frac{\eta^2(t)}{\kappa^2 + (\Delta_c + NU_0\langle\cos^2\tilde{x}\rangle)^2}, \quad (6)$$

where  $\langle\cos^2\tilde{x}\rangle$  is defined as  $\int d\tilde{x} |\tilde{\Psi}(\tilde{x},\tilde{t})|^2 \cos^2\tilde{x}$  and has the meaning of the overlap between the cavity mode intensity and the condensate density distribution. Obviously, it is bounded from above and below,  $0 \leq \langle\cos^2\tilde{x}\rangle \leq 1$ . Equation (6) gives the dependence of the intracavity photon number, i.e., the intracavity optical lattice depth on the condensate. The cavity-pump detuning is shifted by the condensate to an effective value  $\Delta_{\text{eff}} = \Delta_c + NU_0\langle\cos^2\tilde{x}\rangle$ .

Substituting Eq. (6) into Eq. (4), we get a GP equation for the condensate; the most prominent feature of which is that the potential acting on the condensate depends in a highly nonlocal and nonlinear way on the condensate itself. This is to be compared with the nonlinear term in the usual GP equation, the atom-atom interaction, which is nonlinear but local. If this cavity-induced nonlinearity is to exhibit itself apparently, the influence of the condensate on the cavity field should be strong. To this end, it is desirable to have  $\kappa \lesssim NU_0$  (with an appropriate  $\Delta_c$ ). Only under this condition is the condensate able to shift the cavity into or out of resonance with the pump [see Eq. (6)] so as to influence the cavity field drastically. It is worth noting that this condition has been fulfilled with both Fabry-Perot cavities [3,6,7] and ring cavities [11].

Although a brutal integration of Eq. (4) is possible and that captures all the possible atomic modes simultaneously, we would like to introduce the DMA. The advantage of DMA is that it captures the physics and is technically simpler than the full GP equation. To explain the basic idea, let us consider the extremal case  $\omega=0$  and  $g=0$ , i.e., a noninteracting homogeneous condensate. The ground state of the condensate is the zero-momentum state  $|p=0\rangle$ . The effect of the intracavity optical lattice is to diffract this state into the state  $(|p=2k\rangle + |p=-2k\rangle)/\sqrt{2}$  (diffraction into the asymmetrical superposition state is forbidden by the parity symmetry of the potential), which can then be further diffracted into  $(|p=4k\rangle + |p=-4k\rangle)/\sqrt{2}$  (or back into  $|p=0\rangle$ ), and so on. Thus

the dynamics of the system actually confines to some discrete atomic modes. This stimulates us to introduce the DMA.

In the actual case,  $\omega \neq 0$  and  $g \neq 0$ , and the ground state  $\Psi_g(x)$  is not strictly the zero-momentum state. However, usually the length of the condensate is much larger than the period of the optical lattice; thus by the long-range coherence of the condensate and the uncertainty relation, we infer that the momentum distribution of the condensate is well localized around the origin with a width much smaller than  $2k$ . Thus the picture for the noninteracting homogeneous BEC carries over to the actual case as long as in the time scale we are concerned with, the atomic diffraction process dominates other effects caused by the finite trap potential and atom-atom interaction. We can take into account the small but finite momentum spread of the initial state by defining the discrete modes as  $\phi_0 = \Psi_g(x)$ ,  $\phi_1 = \sqrt{2} \cos(2kx) \Psi_g(x)$ ,  $\phi_2 = \sqrt{2} \cos(4kx) \Psi_g(x)$ , and generally for  $n \in \mathbb{N}$ ,  $\phi_n = \sqrt{2} \cos(2nkx) \Psi_g(x)$  [17]. In the momentum representation,  $\phi_n$  is a coherent superposition of the two peaks localized at  $\pm 2nk$ , respectively. For the  $n$ th mode, we introduce the creation (annihilation) operator  $\hat{c}_n^\dagger$  ( $\hat{c}_n$ ) with common boson commutation relations. Note that these mode functions are not strictly orthonormal, so this assignment of commutation relations is a bit problematic. However, as long as the ground state  $\Psi_g(x)$  varies slowly on a length scale of  $\lambda/2$ , the error is negligible.

The DMA assumes that the condensate dynamics is confined in the subspace spanned by  $\{\phi_n\}$ . Numerically, we find that it is enough to cutoff at  $\phi_2$ . Higher modes play a minor role due to the quadratically increasing eigenenergies. Substituting  $\Psi(x) = \sum_{i=0}^2 \hat{c}_i \phi_i(x)$  into Eq. (1) and neglecting the atom-atom interaction, we get the Hamiltonian in the DMA

$$H = 4\omega_r \hat{c}_1^\dagger \hat{c}_1 + 16\omega_r \hat{c}_2^\dagger \hat{c}_2 + \frac{U_0}{4} a^\dagger a [\sqrt{2}(\hat{c}_0^\dagger \hat{c}_1 + \hat{c}_1^\dagger \hat{c}_0) + c_1^\dagger \hat{c}_2 + c_2^\dagger \hat{c}_1 + 2N] + \Delta_c a^\dagger a + \eta(a + a^\dagger) + H_\kappa. \quad (7)$$

In our calculations, we have used the equations  $\int dx \phi_0^* (-\frac{1}{2m} \frac{d^2}{dx^2} + V_{\text{ext}}) \phi_0 \equiv \varepsilon_0$ ,  $\int dx \phi_m^* (-\frac{1}{2m} \frac{d^2}{dx^2} + V_{\text{ext}}) \phi_n \simeq \delta_{mn}(\varepsilon_0 + 4n^2 \omega_r)$ , and  $\int dx \phi_m^* \cos^2(kx) \phi_n \simeq \frac{1}{2} \delta_{mn} + \frac{1}{4} \delta_{m-n,1} [1 + (\sqrt{2}-1) \delta_{m+n,1}]$ , and dropped the constant term proportional to  $\varepsilon_0$ . These equations become exact in the noninteracting homogenous case. In the DMA Hamiltonian, the atom-photon interaction can be interpreted in two ways. For the atoms, they are diffracted between adjacent modes with coupling strengths proportional to the photon number. For the photons, their frequency is renormalized proportional to the interference of the atomic modes.

The atom-atom interaction we neglect contains terms such as  $\hat{c}_1^\dagger \hat{c}_1 \hat{c}_0^\dagger \hat{c}_0$  [18], which shift the energies of the excited modes, and more importantly, it mixes the discrete modes we retain and other modes we discard in a four-wave mixing way. Therefore, the atom-atom interaction impairs the discrete-mode approximation. However, since the energy scale of the atom-atom interaction is on the order of the chemical potential of the condensate  $\mu = (3g\omega/4)^{2/3}$  (in units of  $\omega_r$  in the Thomas-Fermi regime), one can neglect it on a time scale of  $1/\omega_r$  if  $\mu \ll 4$ —the free frequency of the first

excited mode in units of  $\omega_r$ . In the experiment of Brennecke *et al.*,  $4\omega_r \simeq 2\pi \times 15$  kHz, while the chemical potential of the condensate is about  $2\pi \times 2.4$  kHz.

From Hamiltonian (7), by taking the mean-field approximation  $\hat{c}_i \sim \sqrt{NZ_i}$ ,  $a \sim \alpha$ , and integrating out the cavity field, we get the equation of motion for the condensate

$$i \frac{d}{dt} Z = H(n_{\text{ph}}) Z = (H_1 + n_{\text{ph}} H_2) Z, \quad (8)$$

with  $Z = (Z_0, Z_1, Z_2)^T$  and

$$H_1 = \begin{pmatrix} 0 & & \\ & 4 & \\ & & 16 \end{pmatrix}, \quad H_2 = \frac{\tilde{U}_0}{4} \begin{pmatrix} 0 & \sqrt{2} & 0 \\ \sqrt{2} & 0 & 1 \\ 0 & 1 & 0 \end{pmatrix}. \quad (9)$$

The photon number is

$$n_{\text{ph}} = |\alpha|^2 = \frac{\tilde{\eta}^2}{\tilde{\kappa}^2 + (\tilde{\Delta}'_c + 4NZ^\dagger H_2 Z)^2}, \quad (10)$$

where  $\tilde{\Delta}'_c = \tilde{\Delta}_c + N\tilde{U}_0/2$  is the rescaled effective cavity-pump detuning with the condensate in its ground state  $[Z = (1, 0, 0)^T]$ . We would also like to define the general effective cavity-pump detuning  $\tilde{\Delta}_{\text{eff}} = \tilde{\Delta}'_c + 4NZ^\dagger H_2 Z$ . Equation (10) is just Eq. (6) in the discrete-mode approximation.

### III. APPLICATION OF THE FORMALISM

In this section, we apply the formalism developed in Sec. II to two different cases. The first case deals with a constant pump, which acts on the BEC-cavity system abruptly. The evolution of the BEC-cavity system is studied both with the GP equation and the DMA. The second case involves the scenario that the pump is turned on slowly and smoothly. We aim to study the adiabatic evolution of this nonlinear system.

#### A. Constant pump: Validity of the discrete-mode approximation

Assume that initially the BEC is in its ground state and the cavity mode is in the vacuum state. Then at  $t=0$  a beam of laser with constant frequency and constant amplitude is projected onto the cavity. In a time scale of  $1/\kappa$ , the intracavity field and hence the intracavity optical lattice build up, which then diffracts the BEC into higher momentum states. In the position representation, the condensate is deformed by the optical lattice potential. The point is that as the condensate deforms, its overlap with the cavity mode and hence the effective cavity-pump detuning vary, which in turn leads to the variation in the lattice potential. Though matter-wave diffraction by an optical lattice has been extensively studied both theoretically and experimentally since two decades ago [19–23], in all previous works the optical lattice is either static or just a time-dependent parameter. In contrast, here the lattice potential has to be treated as a dynamical variable.

We have simulated the dynamics of the BEC-cavity system with both the GP equation and the discrete-mode approximation. The GP simulations are shown in Figs. 1(a)–1(c) with  $\omega=0.01$  being fixed and  $g=100, 50$ , and  $10$ ,

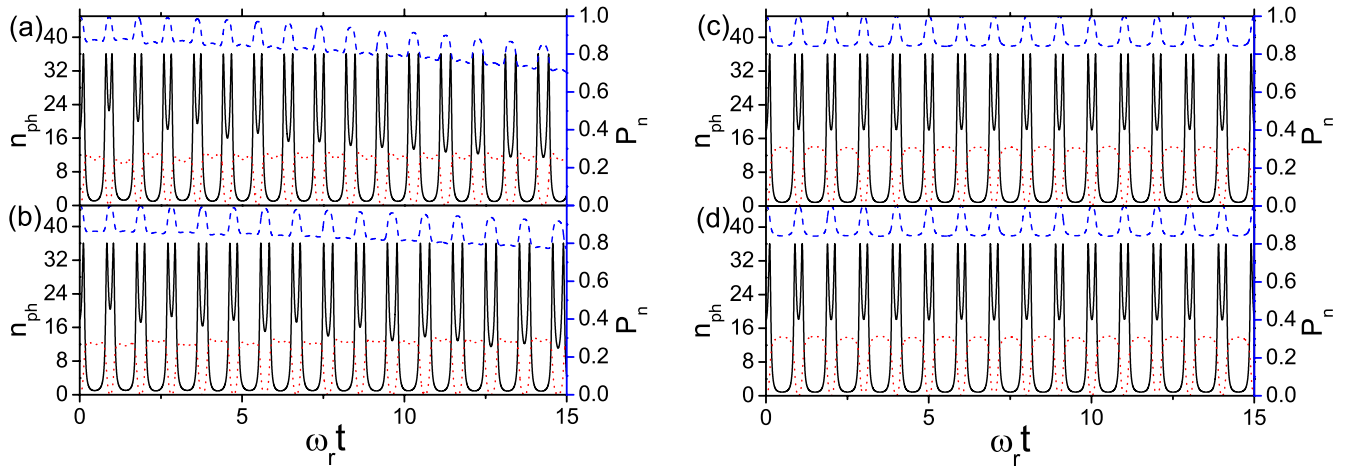


FIG. 1. (Color online) Simulations of the BEC-cavity dynamics [(a)–(c)] with Gross-Pitaevskii equation and (d) with discrete-mode approximation. In each panel, the black solid line is for the photon number, while the blue dashed line and red dotted line are for the normalized populations on the atomic modes  $\phi_0$  and  $\phi_1$ , respectively (populations on the second mode are exaggerated by a factor of 2, whereas that on the third mode are too small and not shown). The parameters are  $N=4.8 \times 10^4$ ,  $\tilde{U}_0=0.25$ ,  $(\tilde{\kappa}, \tilde{\Delta}'_c, \tilde{\eta})=(0.4, 0.4, 2.4) \times 10^3$ ,  $\omega=0.01$ , and  $g=100, 50$ , and  $10$  in (a), (b), and (c), respectively.

respectively. In each figure, we present the evolution of the photon number  $n_{\text{ph}}$  and the normalized populations  $P_n = |\langle \phi_n | \Psi(t) \rangle|^2$  on different atomic modes. In one dimension, the Thomas-Fermi approximation is valid if  $g \gg \sqrt{2\pi}\omega$  [24]. With this criterion, we find that the three cases are all deep in the Thomas-Fermi regime. Thus, the atom-atom interaction plays an important role in determining the ground state of the condensate. In particular, the radius of the condensate is enlarged from  $(1/\omega)^{1/2}$  to  $R_{\text{TF}}=(4g/3\omega)^{1/3}$  (in units of  $\xi=\lambda/2\pi$ ). For all the three cases, we have  $R_{\text{TF}} \gg \pi$ ; therefore the basic condition for DMA is satisfied.

The simulation based on DMA is presented in Fig. 1(d). Note that in DMA, the atom-atom interaction and the initial ground state are irrelevant. Thus, Fig. 1(d) is a common approximation to Figs. 1(a)–1(c). By comparing Fig. 1(d) with Figs. 1(a)–1(c), we see that to a time scale as long as  $\omega_r t=15$ , the discrete-mode approximation agrees with the full GP equation very well. Moreover, the agreement improves as the atom-atom interaction decreases. The DMA recovers the  $g=10$  case [Fig. 1(c)] almost exactly. By examining the difference of Figs. 1(a)–1(c) with Fig. 1(d), we identify two consequences of the atom-atom interaction. First, we see in Figs. 1(a) and 1(b) that as time goes on, the total populations on the discrete modes we take decrease and the time scale of this process increases with decreasing atom-atom interaction. Therefore, it is reasonable to attribute this phenomenon to the atom-atom interaction, which populates the atoms outside the modes we take. Second, the atom-atom interaction shifts up the frequencies of the excited atomic modes and thus shortens the oscillation period of the system [25].

To illustrate the second point, we plot in Fig. 2 the evolution of the effective detuning  $\Delta_{\text{eff}}$  in Figs. 1(a)–1(d). The oscillation of  $\Delta_{\text{eff}}$  is directly related to that of the photon number. We see clearly that the periods in GP simulations are a bit shorter than that in DMA, and the stronger the atom-atom interaction, the more apparent this effect. Figure 2 also

helps us understand the double-peak structure of the photon number line in Fig. 1. Each time  $\Delta_{\text{eff}}$  crosses zero,  $n_{\text{ph}}$  attains its maximal value  $\tilde{\eta}^2/\tilde{\kappa}^2$ .

### B. Slowly varying pump: Breakdown of adiabaticity and optical bistability

In this section, we proceed to consider the scenario that initially the BEC is in its ground state and the cavity mode is in the vacuum state, and subsequently the pump is slowly and smoothly turned on. In contrast to the situation above where the system is exposed suddenly to a finite pump and experience oscillations indefinitely, here we are concerned with the adiabatic following of the self-sustained steady states. By a self-sustained steady state, we mean that the two sides are stationary and consistent with each other, the condensate is in the ground state determined by the optical lat-

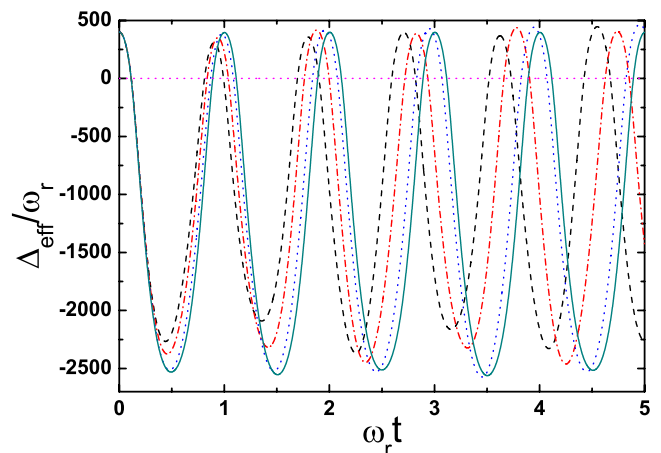


FIG. 2. (Color online) Evolution of the effective detuning  $\Delta_{\text{eff}}$ . The dashed line, dashed dotted line, dotted line, and solid line correspond to Figs. 1(a)–1(d), respectively.

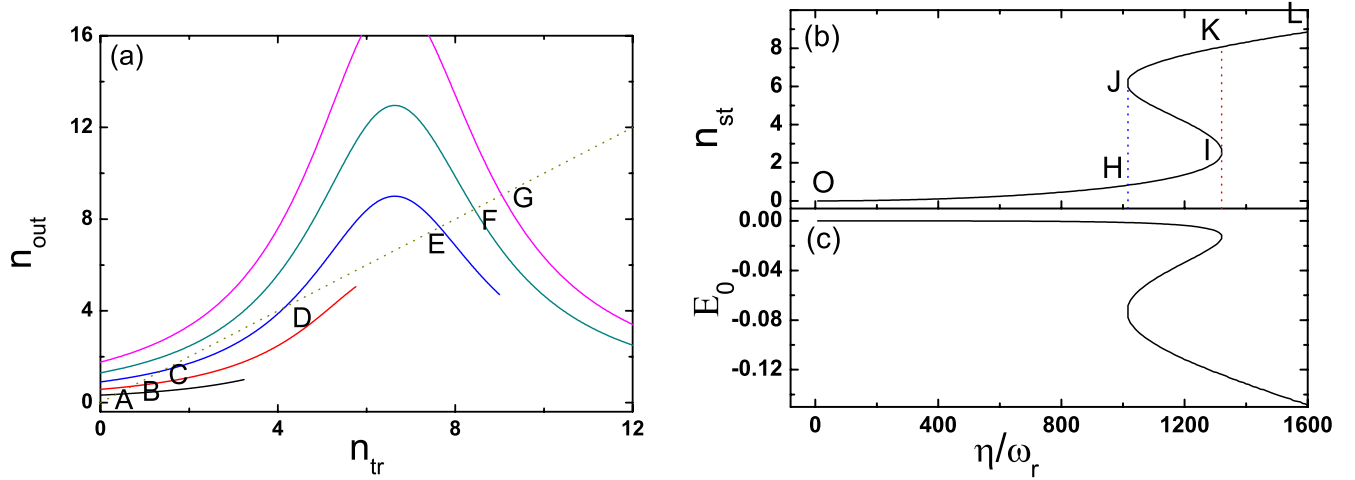


FIG. 3. (Color online) (a) The output photon number  $n_{\text{out}}$  as a function of the trial photon number  $n_{\text{tr}}$ . The intersection points (A–G) of the curves with the diagonal dotted line correspond to steady states. The parameters are  $N=4.8 \times 10^4$ ,  $\tilde{U}_0=0.25$ ,  $(\tilde{\kappa}, \tilde{\Delta}'_c)=(0.4, 1.2) \times 10^3$ , and from bottom to up  $\tilde{\eta}=(0.72, 0.96, 1.20, 1.44, 1.68) \times 10^3$ , respectively. (b) Photon number at steady state  $n_{\text{st}}$  and (c) nonlinear eigenvalue  $E_0$  as a function of the pump strength  $\tilde{\eta}$ . Parameters other than  $\tilde{\eta}$  are the same as in (a). The coordinates of I and J are  $(\tilde{\eta}_1, n_{\text{st}1})=(1296, 2.416)$  and  $(\tilde{\eta}_2, n_{\text{st}2})=(1016, 6.36)$ , respectively.

tice (plus the harmonic trap), and meanwhile the optical lattice (its depth) is determined by the condensate configuration, i.e., fulfilling Eq. (6) or Eq. (10). Naively, it is expected that as long as the pump is ramped up sufficiently slow, the BEC-cavity system will follow the steady states all the way. However, now we are dealing with a nonlinear system and the nonlinearity may give rise to the breakdown of adiabaticity [26–29]. That is what we are interested in.

For our purpose, the key issue is to map out all the possible steady states as the pump strength varies. Although this is a bit difficult (time consuming numerically) in the GP formalism, it can be done very conveniently with DMA. In the framework of DMA, a steady state corresponds to a solution of Eq. (8) such that

$$Z_s(\tilde{t}) = Z_s e^{-iE_0 \tilde{t}}. \quad (11)$$

Or equivalently,

$$H(n_{\text{ph}})Z_s = (H_1 + n_{\text{ph}}H_2)Z_s = E_0 Z_s, \quad (12)$$

which defines a nonlinear eigenvalue problem because the Hamiltonian  $H$  depends on the eigenstate  $Z_s$  through  $n_{\text{ph}}$ . It is impossible to invoke the concepts and tools in linear algebra to solve this problem. Our strategy is to first take an arbitrary trial photon number  $n_{\text{tr}}$ , solve the ground state of the Hamiltonian  $H(n_{\text{tr}})$ ,  $Z_{\text{tr}}$ , and then substitute it into Eq. (10) to get an output photon number  $n_{\text{out}}$ . If  $n_{\text{out}}=n_{\text{tr}}$ , then the solution is self-consistent and a steady state is obtained. Note that  $n_{\text{out}}$ , as a function of  $n_{\text{tr}}$ , is continuous and moreover, it is bounded both from above and below,  $0 < n_{\text{out}} < \tilde{\eta}^2/\tilde{\kappa}^2$ . Therefore, if we scan  $n_{\text{tr}}$  from 0 to  $\tilde{\eta}^2/\tilde{\kappa}^2$  by the principle of continuity, there must be at least one point where  $n_{\text{out}}=n_{\text{tr}}$ . This guarantees the existence of steady-state solutions (clearly the same strategy and arguments apply also in the GP formalism). Furthermore, because of the nonlinearity of the system, the possibility of more than one steady-state solution for a given set of parameters is expected. As observed and argued in Refs.

[26–28], the existence of more eigenvectors than the dimensional of the Hilbert space is unique for nonlinear systems.

In Fig. 3(a), we depict the output photon number  $n_{\text{out}}$  as a function of the trial photon number  $n_{\text{tr}}$  as the pump strength  $\tilde{\eta}$  varies while other parameters are held constant. For each curve, each of its intersections with the dotted line  $n_{\text{out}}=n_{\text{tr}}$  corresponds to a steady state. We see that for  $\tilde{\eta} \leq 960$  and  $\tilde{\eta} \geq 1440$ , there is only one steady-state solution, while in an intermediate range, there can be three (for example,  $\tilde{\eta}=1200$ ). This fact is made more evident in Figs. 3(b) and 3(c), where we plot the photon number at steady state and the nonlinear eigenvalue  $E_0$  as a function of  $\tilde{\eta}$  directly. In the interval  $(\tilde{\eta}_2, \tilde{\eta}_1)=(1016, 1296)$ , each  $\tilde{\eta}$  corresponds to three steady states, and hence three  $n_{\text{st}}$ 's and three  $E_0$ 's. The folded level structure in Fig. 3(c) is similar to the looped level structure in Refs. [26,28].

With these figures as maps, we return to the scenario again. As the pump is slowly ramped up from zero, the BEC-cavity system follows the curve OHI in Fig. 3(b) adiabatically. Things go on like this until the pump exceeds  $\tilde{\eta}_1$ , where the curve terminates. Interpreted in terms of Fig. 3(a), the system first evolves from A to B to C; then at some point C coincides with D, and then they disappear all together. Similar interpretation can be made in terms of Fig. 3(c). As  $\tilde{\eta}$  crosses  $\tilde{\eta}_1$ , the system cannot jump discontinuously from I to K. Therefore, beyond this critical value of the pump, there is no way for the BEC-cavity system to evolve adiabatically anymore, no matter how slow the external pump is varied. We thus expect large amplitude oscillations to appear abruptly as in Fig. 1. This is verified with simulations both based on the GP equation and DMA, as shown in Fig. 4. There we assume that the pump is ramped up and down with a Gaussian profile. Both simulations reveal clearly a two-stage feature of the history of the BEC-cavity system. Before a critical moment  $\tilde{t}_c \sim 40$  (corresponding to  $\tilde{\eta}_c \sim \tilde{\eta}_1$ ), the photon number varies smoothly and coincides with the prediction of DMA perfectly. This indicates that the system

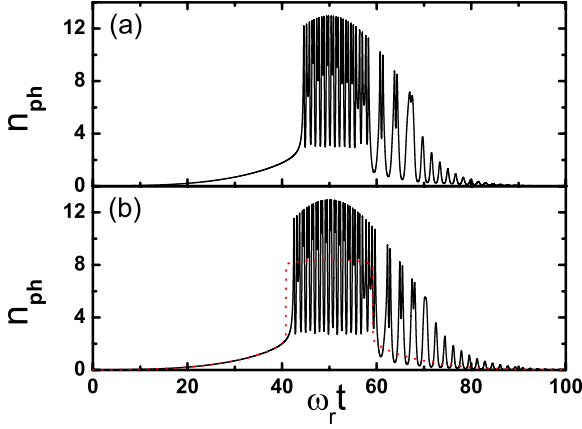


FIG. 4. (Color online) Evolution of the cavity photon number  $n_{\text{ph}}$  as the pump is varied as  $\tilde{\eta}(t) = \tilde{\eta}_{\text{max}} \exp[-(\omega_r t - 50)^2 / \sigma^2]$  with the peak amplitude  $\tilde{\eta}_{\text{max}} = 1440$  and the pulse width  $\sigma = 31.25$ , and other parameters are the same as in Fig. 3. (a) Simulation with the GP equation [ $\omega = 0.01$  and  $g = 10$  as in Fig. 1(c)]; (b) simulation with DMA—the dotted line dictates the photon number of steady states drawn from Fig. 3(b). Note the sharp edges around  $\omega_r t = 40$  in both panels.

evolves adiabatically along the line OHI. However, just across this point, pronounced oscillations with large amplitudes and small periods occur. Experimentally, this sharp transition can be observed by detecting the transmitted light, which is proportional to the intracavity photon number. Note that here the breakdown of adiabaticity is related to the disappearance of a nonlinear eigenstate. This is to be compared with its counterpart in linear systems, which generally results from level crossing. While the latter can be avoided, in principle, the former cannot. In the viewpoint of state preparation, to prepare the system on the line KL, we cannot take the route we take here in the parameter space.

The structure of the curve in Fig. 3(b) reminds us of optical bistability [30]. This motivates us to study the dynamical stability of the steady states. We would like to stress that adiabaticity and stability are two different but closely related issues. Only those steady states which are dynamically stable can be adiabatically evolved [29]. Let  $Z(\tilde{t}) = Z_s(\tilde{t}) + \delta Z(\tilde{t})$ , with  $\delta Z$  being an infinitesimal derivation from the solution  $Z_s$ . Substituting this into the differential Eq. (8) and making use of the fact that  $i \frac{d}{d\tilde{t}} Z_s = [H_1 + H_2 n_{\text{ph}}(Z_s, \bar{Z}_s)] Z_s$ , we get, to the first order in  $\delta Z$ ,

$$i \frac{d}{d\tilde{t}} \delta Z_i = [H_1^{ij} + H_2^{ij} n_{\text{ph}}(Z_s, \bar{Z}_s)] \delta Z_j + H_2^{ij} Z_{sj} \left[ \left( \frac{\partial n_{\text{ph}}}{\partial Z_k} \right)_s \delta Z_k + \left( \frac{\partial n_{\text{ph}}}{\partial \bar{Z}_k} \right)_s \delta \bar{Z}_k \right]. \quad (13)$$

Here the subscript  $s$  means taking value at  $(Z_s, \bar{Z}_s)$ . Assuming

$$\delta Z(\tilde{t}) = e^{-iE_0 \tilde{t}} (u e^{-i\Omega \tilde{t}} - v^* e^{i\Omega^* \tilde{t}}) \quad (14)$$

and substituting this into Eq. (13), we get

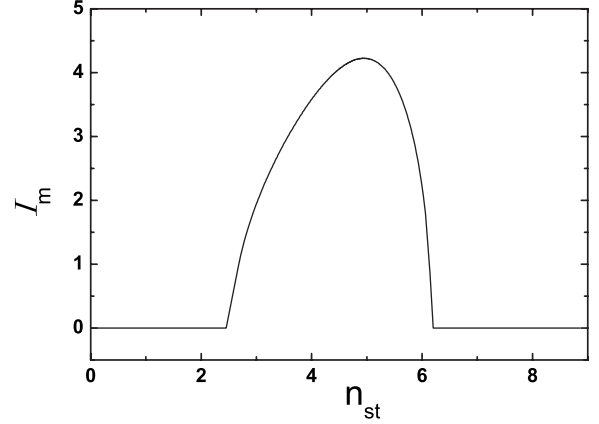


FIG. 5. Maximal imaginary part  $I_m = \max_i \{\text{Im}(\lambda_i)\}$  of the eigenvalues of  $M$ . The points on the curve OHIJKL in Fig. 3(b), which is parametrized with  $n_{\text{st}}$ , are examined. The interval where  $I_m$  is nonzero is  $(n_{\text{st}1}, n_{\text{st}2})$ .

$$M \begin{pmatrix} u \\ v \end{pmatrix} = \Omega \begin{pmatrix} u \\ v \end{pmatrix}, \quad (15)$$

where

$$M = \begin{pmatrix} A + B - E_0 & -B \\ B & -A - B + E_0 \end{pmatrix}. \quad (16)$$

Here the  $3 \times 3$  real matrices  $A$  and  $B$  are defined as

$$A = H_1 + n_{\text{ph}}(Z_s, \bar{Z}_s) H_2,$$

$$B_{ij} = (H_2^{ik} Z_{sk}) \left( \frac{\partial n_{\text{ph}}}{\partial Z_j} \right)_s, \quad 0 \leq i, j, k \leq 2. \quad (17)$$

The dynamical stability of the steady states is determined by the eigenvalues of the matrix  $M$ . If all the eigenvalues are real, the steady state is dynamically stable; otherwise, it is dynamically unstable [31].

In Fig. 5, we examine the stability of the steady states on the curve OHIJKL by plotting the maximal imaginary part  $I_m = \max_i \{\text{Im}(\lambda_i)\}$  of the eigenvalues of  $M$  (as a real matrix, its eigenvalues appear in conjugate pairs). The curve is parametrized with the photon number  $n_{\text{st}}$ . We see that for  $n_{\text{st}} < n_{\text{st}1}$  ( $n_{\text{st}} > n_{\text{st}2}$ ), which corresponds to OHI (JKL), the eigenvalues are all real, and thus steady states on these segments are stable. While for  $n_{\text{st}1} < n_{\text{st}} < n_{\text{st}2}$ , which corresponds to IJ, some eigenvalues are complex, and thus steady states on this segment are unstable. This is consistent with the usual observation that the negative sloped parts are always unstable, though the positive sloped parts are not necessarily stable [30,32]. As noted previously, stability is a prerequisite of adiabaticity. Here, this implies that we can propagate adiabatically the BEC-cavity system along the line OHI (as we do above), but it is not feasible to do that along IJ.

The analysis of stability confirms the possibility of optical bistability in the BEC-cavity system. In previous experiments dealing with a cloud of thermal cold atom gas [3], optical bistability has been discussed and observed, but an

analysis of stability is lacking. If there are some dissipation channels, it may be possible to switch between the upper and lower stable branches and observe the typical hysteresis loop of optical bistability in the BEC-cavity system. Here we can only simulate the coherent behavior of the system, and thus this phenomenon is beyond our means. However, the mechanism underlying optical bistability still manifests itself in the form of breakdown of adiabaticity.

#### IV. CONCLUSIONS

We have investigated the nonlinear dynamics of a BEC-cavity system. This system is characterized by the nonlinearity that the optical lattice acting on the condensate depends on the condensate itself in a highly nonlinear and nonlocal way. By borrowing ideas from atom optics, we develop the discrete-mode approximation (DMA). The philosophy of DMA is that the dynamics of the condensate confines to a series of discrete standing-wave modes. It is numerically verified that in the limit of weak atom-atom interaction, DMA agrees with the full GP equation dynamics perfectly. We focus on the adiabatic evolution of the BEC-cavity system, as the external parameter, the pumping strength slowly varied. The DMA facilitates us to solve the nonlinear eigenstates of the system and analyze their stability. Due to the nonlinearity of the system, the nonlinear energy level can be folded in some parameter regimes. This structure gives rise to both the breakdown of adiabaticity and optical bistability in this system. We conjecture that these two effects are complementary to each other. If the dynamics of the system

is purely coherent, breakdown of adiabaticity will show up; otherwise, if dissipations are strong, coherent oscillations will damp out and the system will settle down to the steady states on the other stable branch, i.e., optical bistability takes the place in the end.

*Note added.* Recently, we became aware of the experimental progress made by Ritter *et al.* [33]. Both coherent dynamics and optical bistability have been confirmed in their experiment. In particular, coherent oscillations of the condensate resulting from the nonadiabatic branch transition (corresponding to our Fig. 4) are observed. However, the transition between the two stable branches is sharp overall, which indicates that dissipation effects are very efficient in their experiment. Potential dissipation channels include atom loss and interaction between the condensate and the normal component, which may damp the coherent oscillations of the condensate. Moreover, since the atom-induced cavity frequency shift depends on the total atom number, atom loss may also influence the dynamics of the system in another way. All these effects deserve further studies.

#### ACKNOWLEDGMENTS

This work was supported by NSF of China under Grant Nos. 10874235, 60525417, and 10775176, and by NK-BRSF of China under Grant Nos. 2009CB930704, 2006CB921400, 2006CB921206, and 2006AA06Z104. J.M.Z. would like to thank J. Ye and S. Ritter for stimulating discussions.

- 
- [1] F. Brennecke, T. Donner, S. Ritter, T. Bourdel, M. Köhl, and T. Esslinger, *Nature (London)* **450**, 268 (2007).
- [2] Y. Colombe, T. Steinmetz, G. Dubois, F. Linke, D. Hunger, and J. Reichel, *Nature (London)* **450**, 272 (2007).
- [3] S. Gupta, K. L. Moore, K. W. Murch, and D. M. Stamper-Kurn, *Phys. Rev. Lett.* **99**, 213601 (2007).
- [4] J. A. Sauer, K. M. Fortier, M. S. Chang, C. D. Hamley, and M. S. Chapman, *Phys. Rev. A* **69**, 051804(R) (2004).
- [5] S. Slama, S. Bux, G. Krenz, C. Zimmermann, and P. W. Courteille, *Phys. Rev. Lett.* **98**, 053603 (2007).
- [6] K. W. Murch, K. L. Moore, S. Gupta, and D. M. Stamper-Kurn, *Nat. Phys.* **4**, 561 (2008).
- [7] F. Brennecke, S. Ritter, T. Donner, and T. Esslinger, *Science* **322**, 235 (2008).
- [8] A. Öttl, S. Ritter, M. Köhl, and T. Esslinger, *Phys. Rev. Lett.* **95**, 090404 (2005); T. Bourdel, T. Donner, S. Ritter, A. Öttl, M. Köhl, and T. Esslinger, *Phys. Rev. A* **73**, 043602 (2006); S. Ritter, A. Öttl, T. Donner, T. Bourdel, M. Köhl, and T. Esslinger, *Phys. Rev. Lett.* **98**, 090402 (2007).
- [9] I. B. Mekhov, C. Maschler, and H. Ritsch, *Nat. Phys.* **3**, 319 (2007).
- [10] W. Chen, D. Meiser, and P. Meystre, *Phys. Rev. A* **75**, 023812 (2007); W. Chen and P. Meystre, e-print arXiv:0811.0045.
- [11] J. Klinner, M. Lindholdt, B. Nagorny, and A. Hemmerich, *Phys. Rev. Lett.* **96**, 023002 (2006); Th. Elsässer, B. Nagorny, and A. Hemmerich, *Phys. Rev. A* **69**, 033403 (2004); B. Nagorny, Th. Elsässer, and A. Hemmerich, *Phys. Rev. Lett.* **91**, 153003 (2003).
- [12] P. Horak, S. M. Barnett, and H. Ritsch, *Phys. Rev. A* **61**, 033609 (2000).
- [13] J. Larson, B. Damski, G. Morigi, and M. Lewenstein, *Phys. Rev. Lett.* **100**, 050401 (2008); J. Larson, S. Fernandez-Vidal, G. Morigi, and M. Lewenstein, *New J. Phys.* **10**, 045002 (2008); J. Larson, G. Morigi, and M. Lewenstein, *Phys. Rev. A* **78**, 023815 (2008).
- [14] J. M. Zhang, W. M. Liu, and D. L. Zhou, *Phys. Rev. A* **78**, 043618 (2008).
- [15] A. Görlitz, J. M. Vogels, A. E. Leanhardt, C. Raman, T. L. Gustavson, J. R. Abo-Shaeer, A. P. Chikkatur, S. Gupta, S. Inouye, T. Rosenband, and W. Ketterle, *Phys. Rev. Lett.* **87**, 130402 (2001).
- [16] C. Maschler and H. Ritsch, *Phys. Rev. Lett.* **95**, 260401 (2005).
- [17] The atom-atom interaction is taken into account implicitly in the definition of atomic modes but not in the dynamics.
- [18] Terms such as  $c_1^\dagger c_1^\dagger c_0 c_0$  are energetically detuned, and thus play a relatively minor role if the chemical potential of the condensate is much smaller than the energy detuning, i.e.,  $\mu = (3g\omega/4)^{2/3} \ll 4$ .
- [19] C. S. Adams, M. Sigel, and J. Mlynek, *Phys. Rep.* **240**, 143

- (1994).
- [20] A. F. Bernhardt and B. W. Shore, *Phys. Rev. A* **23**, 1290 (1981).
- [21] P. L. Gould, G. A. Ruff, and D. E. Pritchard, *Phys. Rev. Lett.* **56**, 827 (1986); P. J. Martin, P. L. Gould, B. G. Oldaker, A. H. Miklich, and D. E. Pritchard, *Phys. Rev. A* **36**, 2495 (1987); P. J. Martin, B. G. Oldaker, A. H. Miklich, and D. E. Pritchard, *Phys. Rev. Lett.* **60**, 515 (1988).
- [22] Yu. B. Ovchinnikov, J. H. Müller, M. R. Doery, E. J. D. Vredenbregt, K. Helmerson, S. L. Rolston, and W. D. Phillips, *Phys. Rev. Lett.* **83**, 284 (1999).
- [23] A. R. Kolovsky and H. J. Korsch, *Phys. Rev. A* **57**, 3763 (1998).
- [24] In one dimension, in contrast to that in three dimension, the weaker the harmonic potential, the better the Thomas-Fermi approximation.
- [25] J. Stenger, S. Inouye, A. P. Chikkatur, D. M. Stamper-Kurn, D. E. Pritchard, and W. Ketterle, *Phys. Rev. Lett.* **82**, 4569 (1999).
- [26] B. Wu and Q. Niu, *Phys. Rev. A* **61**, 023402(R) (2000).
- [27] H. Pu, P. Maenner, W. Zhang, and H. Y. Ling, *Phys. Rev. Lett.* **98**, 050406 (2007).
- [28] E. M. Graefe, H. J. Korsch, and D. Witthaut, *Phys. Rev. A* **73**, 013617 (2006).
- [29] H. Y. Ling, H. Pu, and B. Seaman, *Phys. Rev. Lett.* **93**, 250403 (2004).
- [30] Actually, Fig. 3(b) may also be plotted with  $n_{st}$  versus the maximal photon number  $n_m = \tilde{\eta}^2 / \tilde{\kappa}^2$ . By definition in Eq. (12),  $Z_s$  is a function of  $n_{st}$  and so is  $Z_s^\dagger H_2 Z_s$ , which we denote as  $f(n_{st})$ . To the lowest order,  $f(n_{st})$  is linear in  $n_{st}$ ,  $f(n_{st}) = \beta n_{st}$ . From Eq. (10), we then have  $n_m = n_{st} [1 + (\tilde{\Delta}_c^\dagger + 4N\beta n_{st})^2 / \tilde{\kappa}^2]$ , which can be mapped exactly to the input-output relation in the discussion of dispersive optical bistability; see P. Meystre and M. Sargent III, *Elements of Quantum Optics*, 3rd ed. (Springer-Verlag, Berlin, 1999).
- [31] B. Wu and Q. Niu, *Phys. Rev. A* **64**, 061603(R) (2001).
- [32] K. Ikeda, *Opt. Commun.* **30**, 257 (1979).
- [33] S. Ritter, F. Brennecke, C. Guerlin, K. Baumann, T. Donner, and T. Esslinger, e-print arXiv:0811.3967.